



Published in final edited form as:

J Neuroendocrinol. 2021 December ; 33(12): e13063. doi:10.1111/jne.13063.

Distribution of androgen receptor mRNA in the prepubertal male and female mouse brain

Alexandra L. Cara¹, Emily L. Henson¹, Bethany G. Beekly², Carol F. Elias^{1,2,3}

¹Department of Molecular & Integrative Physiology, University of Michigan.

²Neuroscience Graduate Program, University of Michigan.

³Department of Obstetrics and Gynaecology, University of Michigan, Ann Arbor, Michigan, 48109

Abstract

Androgens are steroid hormones that play a critical role in brain development and sexual maturation by acting upon both androgen receptors (AR), and estrogen receptors (ER α/β) after aromatization. The contribution of estrogens from aromatized androgens in brain development and the central regulation of metabolism, reproduction, and behavior is well defined, but the role of androgens acting on AR has been unappreciated. Here we map the sex specific expression of *Ar* in the adult and developing mouse brain. Postnatal days (PND) 12 and 21 were used to target a critical window of prepubertal development. Consistent with previous literature in adults, sex-specific differences in *Ar* expression were most profound in the bed nucleus of the stria terminalis (BST), medial amygdala (MEA), and medial preoptic area (MPO). *Ar* expression was also high in these areas in PND 12 and 21 of both sexes. In addition, we describe extra-hypothalamic and extra-limbic areas which show moderate, consistent, and similar *Ar* expression in both sexes at both prepubertal time points. Briefly, *Ar* expression was observed in olfactory areas of the cerebral cortex, in the hippocampus, several thalamic nuclei, and cranial nerve nuclei involved in autonomic sensory and motor function. To further characterize forebrain populations of *Ar* expressing neurons and determine whether they also coexpress estrogen receptors, we examined expression of *Ar*, *Esr1*, and *Esr2* in prepubertal mice in selected nuclei. We found populations of neurons in the BST, MEA, and MPO that coexpress *Ar*, but not *Esr1* or *Esr2*, while others express a combination of the three receptors. Our findings indicate that various brain areas express *Ar* during prepubertal development and may play an important role in female neuronal development and physiology.

Keywords

sex differences; gonadal steroids; postnatal development; puberty

Corresponding author: Dr. Carol Elias, PhD, Department of Molecular & Integrative Physiology, University of Michigan, Ann Arbor, MI, 48109, Tel: 734-647-2801, cfelias@umich.edu.

Author contribution: ALC conducted experiments, analyzed data, and wrote manuscript. ELH and BGB conducted experiments. CFE analyzed data and edited manuscript.

Conflict of interest disclosure: The authors have no conflict of interest to declare.

Introduction

Gonadal steroids, including androgens and estrogens, play a dominant role in the development of sex differences in the brain. During male embryonic development, expression of the *Sry* gene located on the Y chromosome leads to differentiation of bipotential gonads into testes, which begin secreting testosterone¹⁻⁴. Embryonic testosterone is locally converted to estradiol by the enzyme P450 aromatase (*CYP19A1*)⁵⁻⁷, which acts to masculinize and defeminize specific brain nuclei via estrogen receptor alpha (ER α) and estrogen receptor beta (ER β)⁸⁻¹¹. Both effects take place during the organizational window of development¹²⁻¹⁴, when the bipotential brain is most sensitive to the organizational effect of gonadal steroids. Developing females, which lack *Sry*, do not develop testes or produce testosterone, and are protected from maternal estradiol by the presence of alpha-fetoprotein *in utero*, and therefore differentiate toward a feminized brain^{15,16}. As a result, several adult brain sites display gonadal steroid-dependent sexual dimorphism¹⁷⁻²⁰.

During puberty, increased activity of hypothalamic gonadotropin releasing hormone (GnRH) neurons drives pituitary synthesis and release of gonadotropins, which induce gonadal steroid secretion and production of mature gametes²¹. Testosterone activates developmentally programmed brain circuits to generate male specific behaviors, while cyclical ovarian steroids have a similar role in females²². Circulating levels of androgens are higher in males during and after completion of puberty²³⁻²⁵, while very low levels of androgens are detected during the prepubertal stage in both sexes. In the hypothalamus, however, androgen receptor immunoreactivity (AR-ir) is observed throughout postnatal development in rodents. AR-ir is higher in male mice at postnatal day 5, but comparable at 15 days of age, when increasing numbers of female neurons show AR-ir²⁶. This is highly relevant as the prepubertal window between postnatal days 12 and 22 accounts for the greatest differences in temporal gene expression^{27,28} indicating that active neurodevelopmental changes occur prior to puberty and the activation of the hypothalamic-pituitary-gonadal (HPG) axis, when circulating gonadal steroids are low, particularly in females.

The requirement of gonadal steroids and sexual dimorphism in specific brain nuclei for reproduction has been widely demonstrated^{29,30}, but the same cannot be said of nonreproductive sex-dependent or sex-associated brain responses and function. Among them, emotion, motivation, addiction, and energy balance are well-defined³¹. Notably, sex is one of the most relevant risk factors for a variety of psychiatric and neurologic disorders, most of which show clinical onset in peripubertal stages³². Whether this is a direct effect of developmental testosterone is not clear. In both sexes, many adult brain areas outside reproductive centers are androgen sensitive and express AR³³, but the distribution of *Ar* expression in male and female brain during the prepubertal time window has been poorly defined.

In this study, we performed a comprehensive analysis of *Ar* expression in the mouse brain, expanding upon previous descriptions^{26,34-37} to include all main subdivisions (e.g., neocortex, thalamus, brainstem, circumventricular organs) in both sexes. In addition, we mapped the distribution of *Ar* expression in the developing brain, specifically at postnatal

days 12 and 21, which frame a critical window of pubertal development^{27,28}. Finally, we evaluated whether *Ar* is coexpressed with *Esr1* and/or *Esr2* in prepubertal forebrain neurons to gain insight into the nuclei that express *Ar* but not genomic acting ERs. Our data provides a greater in-depth anatomical map of reproductive and non-reproductive sites of androgen action in the male and female mouse brain during pubertal transition.

Methods

Animal Ethics

All research animals were acquired, used, and maintained in accordance with the National Research Council *Guide for the Care and Use of Laboratory Animals*³⁸, the US Public Health Service's Policy on Humane Care and Use of Laboratory Animals, and Guide for the Care and Use of Laboratory Animals, as well as federal, state, and local laws. Procedures and protocols were approved by the University of Michigan Committee on Use and Care of Animals (IACUC, Animal Protocol: PRO8712).

Animals

C57BL/6J (JAX[®] mice, stock #000664), mice were housed in an Association for Assessment and Accreditation of Laboratory Animal Care (AAALAC) accredited facility at the University of Michigan Medical School. Mice were housed in a 12:12 light/dark cycle environment with controlled temperature (21–23°C) and humidity (30–70%). Mice were provided water ad libitum and were fed a phytoestrogen-reduced diet (16% protein, 4.0% fat, 48.5% carbohydrate, Teklad 2916 irradiated global rodent diet, Envigo) or a phytoestrogen-reduced, higher protein and fat diet (19% protein, 9% fat, 44.9% carbohydrate, Teklad 2919 irradiated global rodent diet, Envigo) for breeding and lactating females. Phytoestrogen-reduced diets were used to avoid any effects of exogenous dietary estrogens on AR expression in experimental mice. Adult male mice were single housed at least one week prior to euthanasia to control for housing status, which may impact testosterone levels³⁹, and androgen-regulated AR expression^{36,37}. Adult female mice (group housed) were euthanized during diestrus, after completing at least two estrous cycles. Cycle stage was determined by vaginal lavage with predominately leukocytes⁴⁰ and confirmed by uterine weight below 100 mg⁴¹.

Sample size was 5–9 animals per sex and per age group (PND 12, PND 21, and adult).

Tissue preparation

Adult (postnatal day (PND) 56–70) and PND 21 mice were deeply anesthetized with isoflurane and transcardially perfused with diethyl pyrocarbonate (DEPC)-treated 0.1M PBS until liver and lungs cleared (about 1 minute), followed by 10% neutral buffered formalin (NBF) for 10 minutes. Brains were dissected and postfixed for 2 h, then transferred to 20% sucrose in DEPC-treated 0.1M PBS overnight for cryoprotection. PND 12 mice were anesthetized with isoflurane and euthanized by decapitation. Brains were dissected and fixed in 10% NBF for 4 h, then transferred to 20% sucrose in 10% NBF for 48–72 h at 4°C. PND 12 and PND 21 brains were embedded in optimal cutting temperature (OCT) compound, frozen on dry ice, and stored at –80°C. Brains from PND 12 and 21 mice were sectioned

at 30 μm thickness on the frontal plane into 4–5 series on a cryostat (Leica CM 3050S). Sections were directly collected onto SuperFrost Plus slides (Fisher Scientific) and stored at -20°C . Adult brains were sectioned at 30 μm thickness on the frontal plane into 5 series on a freezing microtome (Leica SM 2010R). Sections were stored at -20°C in DEPC-treated cryoprotectant.

Immunohistochemistry

AR immunoreactivity was visualized using a modified tyramide signal amplification (TSA) method previously described⁴². Brain sections were rinsed with 0.1M PBS, incubated in 0.6% hydrogen peroxide for 30 min, rinsed with 0.1M PBS, then blocked with 3% normal donkey serum with 0.25% Triton-X-100 for 1 h at room temperature. Sections were incubated overnight with rabbit anti-AR antibody (1:200, AbCam [EPR1535(2)], Cat #ab133273, RRID: AB_11156085). A series with no primary antibody was included as a negative control (Figure 1A-B). Sections were rinsed with 0.1M PBS and then incubated for 1 h with biotinylated donkey anti-rabbit IgG (1:500, Jackson ImmunoResearch Laboratories, Cat #711-065-152, RRID: AB_2340593), followed by incubation in avidin-biotin (AB) solution in 0.1M PBS (1:1000, Vector Laboratories) for 1 h. Next, sections were incubated in biotinylated tyramide (1:250, Perkin Elmer) with 0.009% hydrogen peroxide for 10 min, followed by incubation with streptavidin-conjugated AlexaFluor 594 (1:1000, Invitrogen, ThermoFisher) for 1 h. Sections were mounted onto gelatin-coated slides and coverslipped with ProLong Gold Antifade mounting medium (Invitrogen, ThermoFisher).

In situ hybridization

Adult brain sections were mounted onto Superfrost Plus slides (Fisher Scientific) in DEPC-treated 0.1M PBS, air dried overnight at room temperature, and stored at -20°C . For pretreatment, slides were thawed at room temperature for 15–20 min, then fixed with 10% NBF for 15 min. Slides were rinsed with DEPC-treated PBS, then dehydrated with increasing concentrations of ethanol and cleared with xylene. Slides were rehydrated, boiled in sodium citrate (0.01M sodium citrate, pH 6.0 in DEPC- H_2O) in a microwave for 10 min, dehydrated, and air dried for 30 min at room temperature.

To generate a ^{35}S -labelled *Ar* cRNA riboprobe, a cDNA template was first generated by RT-PCR amplification using cDNA obtained from whole mouse hypothalamic RNA (TRIzol Reagent, Ambion, Life Technologies) and the primer pairs FOR 5' CAACCAGATTCCTTTGCTGCC 3' and REV 5' GAGCTTGGTGAGCTGGTAGAA 3' (NCBI accession number NM_013476.4, *M. musculus* androgen receptor (*Ar*), mRNA, target region 3042–3551, product length 510 bp). Linear template PCR products were gel purified according to the manufacturer's protocol (QIAquick Gel Extraction Kit, 28706, Qiagen). To generate an antisense cRNA ^{35}S -*Ar* riboprobe by *in vitro* transcription, the linear template was incubated with ^{35}S -UTP (UTP α S, Perkin Elmer) and T7 RNA polymerase according to the manufacturer's protocol (Promega). A control sense cRNA ^{35}S -*Ar* riboprobe was generated with T3 RNA polymerase using the same protocol (Figure 1C-D). Riboprobes were diluted to 10^6 cpm/mL in hybridization buffer (50% formamide, 10mM Tris-HCl, pH 8.0 (Invitrogen), 5mg tRNA, 10mM dithiothreitol (DTT), 10% dextran sulfate, 0.3M NaCl, 1mM EDTA, 1x Denhardt's Solution, 0.1% SDS, 0.1% sodium

thiosulfate). Hybridization solution was applied to slides, which were coverslipped and incubated overnight at 57°C. The following morning, slides were treated with RNase A (Roche Applied Bioscience) for 30 min, then treated with a series of high stringency washes in sodium chloride-sodium citrate buffer (SSC). Slides were dehydrated, air dried, then placed into an X-ray film cassette with Biomax MR film (Carestream) for 1–2 days. Slides were dipped in NTB autoradiographic emulsion (Kodak, VWR), dried, and stored at 4°C in foil-wrapped slide boxes for 5 days per 1 day of film exposure. Slides were developed with GBX (Carestream Dental) developer and fixer, then dehydrated with graded ethanol, cleared with xylene, and coverslipped with DPX mounting media (Electron Microscopy Sciences).

To generate neuroanatomical references, slides with adjacent sections of PND 12 and 21 male and female brains were dipped in 0.25% thionin for 45 s, quickly rinsed in water, dehydrated in increasing concentration of ethanol, and cleared in xylene. Slides were coverslipped with DPX mounting media.

Fluorescent *In Situ* Hybridization

For fluorescent ISH, PND 12 and PND 21 mice were deeply anesthetized with isoflurane and euthanized by decapitation. Brains were rapidly removed, embedded in optimal cutting temperature (OCT) compound, frozen on dry ice, and stored at –80°C. Brains were sectioned at 16 µm thickness on the frontal plane into 5 series on a cryostat (Leica CM 3050S). Sections were directly collected onto SuperFrost Excell slides (Fisher Scientific) and stored at –80°C. Tissue sections were fixed in 10% NBF for 15 min and then dehydrated with graded ethanol. An RNAscope™ Multiplex Fluorescent Assay v2 (Advanced Cell Diagnostics, ACD) kit was used for blocking, hybridization, and amplification steps, following manufacturer's instructions. Briefly, endogenous peroxidase activity was blocked with H₂O₂ for 10 min, washed in DEPC-treated water, and then sections were gently digested with Protease IV for 30 min at room temperature. Sections were then incubated with probes targeting *M. musculus Ar* (ACD Cat #316991-C2, NCBI Accession # NM_013476.3, target region: 1432–2422), *Esr1* (ACD Cat # 478201-C3, NCBI Accession # NM_007956.5, target region: 678–1723), and *Esr2* (ACD Cat # 316121, NCBI Accession # NM_207707, target region: 424–1875) for 2 h at 40°C. Following hybridization, probes were labelled via tyramide signal amplification with fluorescent dyes (Opal520, OpalCy3, or OpalCy5, Akoya Biosciences). Sections were counterstained with DAPI, then coverslipped with Prolong Gold antifade mounting media. Probes have been validated by ACD, but we performed an additional control by analyzing previously described distribution of all three genes, and our own *in situ* hybridization using radioisotopes.

Microscopy and Image Acquisition

Digital images were acquired using an Axio Imager M2 (Carl Zeiss) with a digital camera (AxioCam, Zeiss) using Zen Pro 2 software (Zeiss). Digital images of fluorescent ISH were acquired using a Nikon A1si inverted confocal microscope and Nikon Elements software at the University of Michigan BRCF Microscopy Core. Photomicrographs of films were acquired using a SteREO Discovery.V8 stereomicroscope with a digital camera (AxioCam, Carl Zeiss), using the same magnification, illumination, and exposure time for each image.

Dark field photomicrographs for silver grains (hybridization signal) were acquired using the same illumination and exposure time for each section, at 10× magnification.

Illustration

Adobe Photoshop software (Adobe Creative Cloud) was used to prepare digital images, including adjusting resolution to 300 dpi, adjustment of image size, addition of annotation and labels, conversion to greyscale, unsharp mask, and levels. Uniform adjustments were made to every image. Mouse brain coordinates were estimated from Paxinos and Franklin's Mouse Brain in Stereotaxic Coordinates atlas⁴³. Abbreviations are based on the Allen Mouse Brain Atlas (postnatal day 56, coronal reference atlas, Allen Institute for Brain Science, Allen Mouse Brain Atlas, <http://mouse.brain-map.org/static/atlas>).

Data Analysis

Estimation of hybridization signal was obtained by analysis of integrated optical density (IOD) using ImageJ software (NIH, <http://rsb.info.nih.gov/ij>) as previously described^{44,45}. Briefly, IOD values were calculated as the total IOD of a constant region of interest (ROI) after subtracting background intensity. Quantification of *Ar* silver grain IOD was performed in one 30-µm thick section, on one hemisphere of each animal ($n = 5-9$ /group), at approximately the same rostrocaudal level. Qualitative analysis was subjective based on relative expression (e.g., highest expression = +++++, and lowest expression = +), and was performed by two independent evaluators. Co-expression of *Ar*, *Esr1*, and *Esr2* in male and female PND 12 and PND 21 mice was evaluated in one 16-µm thick section, on one hemisphere of each animal. Due to the punctate nature of the fluorescent signal and lack of definition of cellular borders, the quantification reflects only an estimation of co-expression relative to total number of *Ar* expressing cells. Only forebrain sites with clear expression of all three genes were quantified.

Statistics

Data are reported as mean ± standard error of the mean (SEM). Analysis was performed using GraphPad Prism software (Version 8). Normal distribution of data was analyzed using Shapiro-Wilk test (significance alpha 0.05). Unpaired *t* test with Welch's correction was used for normally distributed data, and Mann-Whitney nonparametric test was used for non-normally distributed data, to analyze IOD. Exact *P* values are reported and statistical significance is defined as $P < 0.05$.

Results

Distribution of *Ar* mRNA in adult mouse brain

Ar mRNA expression was visualized using in situ hybridization histochemistry. Hybridization signal on autoradiographic film was evaluated in male and female brain sections ($n = 5-9$ /sex, Figure 2A). Adult brains were systematically examined and compared with published data as an initial control^{26,36,37}. Analysis of AR immunoreactivity (AR-ir) was also performed as a control for areas that had not been fully described in previous publications ($n = 3-4$ /sex, Figure 3).

Patterns of hybridization signal were similar between sexes in several subdivisions of the cerebral cortex, including the motor (MO), piriform (PIR), and anterior cingulate (ACA) (Table 1). In the hippocampal formation, highest expression was observed in Field CA1 and CA2 (Figure 2A, Bregma -1.34 through -3.52 mm), and lowest expression in the entorhinal area (ENT). As previously described for AR-ir³⁵⁻³⁷, several cortical subplate and cerebral nuclei displayed apparent sex differences. The lateral septal nucleus (caudodorsal and rostroventral subdivisions, LSc and LStr) (Figure 2A, Bregma $+0.62$, $+0.14$, -0.22 mm), bed nucleus of the stria terminalis (principal, BSTpr) (Figure 2A, Bregma -0.22 mm), posterodorsal medial amygdalar nucleus (MEApd, Figure 2A, Bregma -1.34 mm), and posterior amygdala (PA, Figure 2A, Bregma -2.46 mm) showed higher *Ar* mRNA levels in males. The cortical amygdalar area (COA) displayed high *Ar* mRNA in both sexes (Table 1).

The thalamus and subthalamus contained low to moderate *Ar* hybridization signal. Conspicuous expression was observed in the paraventricular (PVT), medial geniculate (MG), and subthalamic nuclei (STN) in both sexes (Figure 2A, Bregma -1.34 to -3.52 , Table 1).

Hypothalamic AR-ir expression is fairly well characterized in adult mice, and *Ar* hybridization signal was consistent with previous descriptions^{26,34,35,37}. In brief, highest expression was seen in the medial preoptic area (MPO, Figure 2A, Bregma $+0.14$ mm), arcuate nucleus (ARH), ventrolateral subdivision of the ventromedial hypothalamic nucleus (VMHvl, Figure 2A, Bregma -1.34 mm), and ventral premammillary nucleus (PMv, Figure 2A, Bregma -2.46 mm). Sex differences were apparent in the suprachiasmatic nucleus (SCH) and ARH, with expression higher in male mice. Higher *Ar* hybridization signal was also apparent in the periventricular (PV) and dorsomedial (DMH) nuclei of the hypothalamus in males. The tuberal nucleus (TU) displayed low *Ar* expression, and the paraventricular hypothalamic nucleus (PVH) displayed very low expression in both sexes (Table 1). The supramammillary nucleus (SUM) was observed to have an apparent sex difference, with females exhibiting very low expression, and males with higher but still low *Ar* mRNA (Table 1).

In the midbrain, *Ar* mRNA was low in both sexes, and mainly observed in the periaqueductal gray (ventrolateral column, PAGvl) and dorsal raphe nucleus (DR, Figure 2A, Bregma -3.52 and -5.02 mm). Very low expression was also observed in the ventral tegmental area (VTA) and red nucleus (RN) (Table 1).

In the pons and medulla, low *Ar* mRNA expression was observed in the dorsal tegmental (DTN), facial motor (VII), hypoglossal (XII), and dorsal motor nucleus of the vagus nerve (DMX) in both sexes (Figure 2A, Bregma -5.02 mm). Very low hybridization signal was observed in the parabrachial nucleus (PB) and pontine reticular nucleus (PRN, Table 1). *Ar* mRNA was also detected in the nucleus ambiguus (AMB, Figure 2A, Bregma -7.08 mm), and nucleus of the solitary tract (NTS, Figure 1A, Bregma -7.48 mm) of both sexes, while the cochlear (CN) and vestibular nuclei (VNC) displayed very low signal in males, but not in females (Table 1).

In circumventricular organs, we observed very low to low *Ar* hybridization signal in the subfornical organ (SFO) and area postrema (AP) of both sexes (Table 1).

AR-immunoreactivity in adult mouse brain

In the adult brain, our findings thoroughly replicate previous reports by different groups^{26,34,36,37}. In brief, high AR-ir was observed in the BSTpr, MPO, VMHvl, PMv, and MEApd. In addition, and in agreement with *Ar* mRNA distribution, we found moderate to low AR-ir in the PIR, ACA (Figure 3A), CA1 and CA2 (Figure 3B), septohippocampal nucleus (SH), LSc (Figure 3C), PVT (Figure 3D), subparaventricular zone (SBPV, Figure 3E), PA, PAGvl (Figure 3F), DTN (laterodorsal), and many nuclei of the cranial nerves, including the principal sensory nucleus of the trigeminal nerve (PSV), VII, and medial vestibular nucleus (MV, Figure 3G). Scattered AR-ir was also observed in the SFO (Figure 3H) and AP.

Prepubertal distribution of *Ar* mRNA

Ar mRNA expression was analyzed in two developmental prepubertal stages, PND 12 and 21 ($n = 5-9/\text{sex/age}$, Figure 2B-C). In the cerebral cortex, both male and female mice at PND 12 and PND 21 showed consistent and similar expression between sexes (Table 1). The anterior olfactory nucleus (AON) displayed moderate *Ar* hybridization signal, while the taenia tecta (TT), PIR, and ACA displayed low *Ar* hybridization signal (Figure 4A-D). The endopiriform (EP) and MO showed very low *Ar* hybridization signal in PND 12 and PND 21 mice (Table 1).

In the hippocampal formation, expression level of *Ar* mRNA in prepubertal mice was similar to that observed in adults. Briefly, expression of *Ar* mRNA in both male and female mice was detected in the induseum griseum (IG, Figure 4E-F), CA1, CA2 (Figure 4G-H), and presubiculum/subiculum (PRE/SUB). Higher expression was observed in CA1 and CA2, while lower expression was found in Field CA3 (CA3, Table 1). In the dentate gyrus (DG), lower expression was observed in PND 12 of male and female mice. The ENT displayed moderate expression at PND 12 in male and females, but expression decreased by PND 21.

Cortical subplate and cerebral nuclei also exhibited consistent *Ar* hybridization signal in prepubertal mice in the SH (Figure 4E-F) and PA. The LSc displayed moderate expression in PND 12 (Figure 5A-C), and PND 21 (Figure 5D-F). *Ar* hybridization signal was not different between sexes at PND 12 or PND 21 in the LSc (Figure 5C,F). The BSTpr showed similar levels between sexes at PND 12 and PND 21 between sexes (Figure 5G-L). The MEApd showed similar pattern of *Ar* expression in between sexes at PND 12 and PND 21 (Table 1). *Ar* mRNA in the COA was also similar between sexes, with low expression at PND 12, increasing to high expression by PND 21 (Table 1).

In thalamic nuclei, moderate to high levels of *Ar* hybridization signal was observed in the PVT (Figure 6A-B), the nucleus of reuniens (RE, Figure 6C-D), the ventral posterior complex nuclei (VP, Figure 6E-F), the STN (Figure 6G-H) and the MG (Table 1). No difference between sexes and prepubertal ages was apparent.

In the hypothalamus, the MPO and anteroventral periventricular nucleus (AVPV) showed similar levels of *Ar* in both sexes at PND 12 and PND 21 (Table 1). The SCH had similar levels of *Ar* at PND 12 in both sexes (Figure 7A-C, E-G), however, expression increased in male mice at PND 21 (Figure 7G). The SBPV, although apparently higher in males, was not significantly different when comparing sexes at both prepubertal ages (Figure 7D, H). The PMv showed no difference between sexes at PND 12 or PND 21 (Figure 7I-K, M-O). In the dorsal premammillary nucleus (PMd), *Ar* mRNA levels were low to moderate, and no difference between sexes or ages was observed (Figure 7L, P). The SUM displayed low *Ar* mRNA expression in both sexes at PND 12, and low expression in males and very low expression in females at PND 21 (Table 1). The TU exhibited no detectable *Ar* hybridization signal at PND 12, but low signal was detected at PND 21 (Table 1). The PVH had no detectable *Ar* hybridization signal at either PND 12 or 21 (Table 1).

In the midbrain, expression of *Ar* hybridization signal was low to very low. The PAG showed low expression, which was consistent between sexes, particularly in the caudal ventrolateral column (PAGvl, Figure 8A-B, Table 1). The DR also showed a low to very low level of *Ar* mRNA expression in PND 12 and PND 21 mice (Table 1).

In the pons and medulla, the DTN showed consistent, moderate expression in both sexes and in both prepubertal ages (Figure 8A-B, Table 1). Low *Ar* mRNA expression was detected in the superior olivary complex (SOC, Figure 8C-D), the VII (Figure 8E-F), the VNC, and the CN (Table 1) in both prepubertal stages of both sexes. Low to moderate *Ar* expression was observed in the AMB (Figure 8G-H), the DMX and the XII (Figure 8I-J) in males and females. Very low to low levels of *Ar* mRNA were detected in the PRN and the PSV (Table 1).

In circumventricular organs, *Ar* mRNA expression was low to very low in the SFO and AP of both sexes at PND 12 and PND 21 (Table 1).

***Ar* mRNA expression overlaps with *Esr1* and/or *Esr2* in specific forebrain nuclei of prepubertal mice**

We further mapped forebrain sites expressing *Ar*, *Esr1*, and *Esr2*. Because this prepubertal window shows high activity of gene transcription^{27,28}, we focused on sex steroid receptors with well-defined genomic actions. We examined co-expression of *Ar* with *Esr1* and/or *Esr2* also due to their well described role in masculinization of the male brain during development⁴⁶⁻⁴⁸, and the major role they play in female pubertal development⁴⁹. Patterns of *Ar* hybridization signal using a commercial probe (ACD) for fluorescent *in situ* hybridization were similar to our ³⁵S-*Ar* riboprobe. Anatomical distribution of *Esr1* and *Esr2* was consistent with previous reports in adults^{9,26,50,51}. Briefly, we observed a heterogeneous mix of subsets of cells expressing either all three receptors, a combination of two, or only *Ar*, *Esr1*, or *Esr2* in the BSTpr, the MEApd, and the MPO.

In the BSTpr (Figure 9A-D) of PND 12 males, about 20% of *Ar* positive cells co-expressed *Esr1*, ~8% co-expressed *Esr2*, and ~3% expressed all three transcripts. The BSTpr of PND 12 females had ~6% co-expression of *Ar* and *Esr1*, ~12% *Ar* and *Esr2*, and ~1% co-expression of all three transcripts. At PND 21, there was an increase in the approximate

co-expression of *Ar* with *Esr1* and *Esr2* in both sexes. PND 21 males and females showed about 93% co-expression of *Ar* and *Esr1*. PND 21 males had ~98% co-expression of *Ar* and *Esr2*, and ~90% of *Ar* positive cells expressing all three transcripts in the BSTpr. PND 21 females, however, displayed about 50% co-expression between *Ar* and *Esr1*, and both *Esr1* and *Esr2*.

In the MEApd (Figure 9E-H) of PND 12 males, overlap of *Ar* with *Esr1* was abundant (~92%), but co-expression of *Ar* with only *Esr2*, or both *Esr1* and *Esr2* was more limited (~5%). PND 12 females displayed lower co-expression compared to males in the MEApd, with ~30% co-expressing *Ar* and *Esr1*, ~5% co-expressing *Ar* and *Esr2*, and only ~2% expressing all three transcripts. At PND 21, both sexes displayed high co-expression of *Ar* and *Esr1* (about 90%). PND 21 males had lower co-expression between *Ar* and *Esr2* and all three transcripts (~15%) compared to PND 21 females (~35% between *Ar* and *Esr2*, and all three transcripts).

The MPO (Figure 9I-L) displayed a higher percentage of overlap between *Ar* and *Esr1* in males compared to females. In PND 12 males, about 80% of *Ar* expressing cells co-expressed *Esr1*, compared to about 45% in PND 12 females. At PND 21, males displayed ~92% of co-expression between *Ar* and *Esr1*, while about 80% of *Ar* positive neurons in females co-expressed *Esr1*. Co-expression between *Ar* and *Esr2*, and *Ar* with both *Esr1* and *Esr2* was much lower in both sexes at both developmental time points. Co-expression between *Ar* and *Esr2*, and all three transcripts at PND 12 was approximately 10% in males, and 5% in females. At PND 21 in both sexes, co-expression was between 2–3% between *Ar* and *Esr2*, and all three transcripts.

In the SCH (Figure 9M-P), however, very little *Esr1* expression was observed, and therefore, *Ar* neurons co-expressing *Esr1* were rare. Co-expression between *Ar* and *Esr1* was around 15% in males. Additional experiments will be necessary to define the specific subsets of neurons and their role in postnatal development in each brain nucleus expressing all three receptors.

Discussion

In this study, we describe the expression of *Ar* mRNA in the brain of adult and two prepubertal time points of male and female mice. We show that at PND 12 and 21, before the activation of the HPG axis, many brain nuclei express high levels of *Ar* in both sexes. Additionally, we highlight specific forebrain nuclei and subpopulations of *Ar* expressing neurons that co-express *Esr1* and/or *Esr2*. We focused on the genomic actions of sex steroid receptors due to their well described role in masculinization of the male brain during prenatal development^{46,47}, and in female pubertal development and fertility^{49,52}. Further studies will be necessary to evaluate the co-expression of the three nuclear receptors in the entire brain and if the identified brain sites express alternative estrogen receptors (e.g., G protein-coupled ER), or the enzyme aromatase during this window of prepubertal development.

Systematic characterization of AR expression during prepubertal development is essential for understanding how androgens can shape brain organization and activation of neural circuits. While circulating androgens are low in the prepubertal period, we show that *Ar* is highly expressed in many areas of the brain in both sexes during this time window. The exact role of AR in brain development in general, and in specific neuronal subpopulations is not well described. It has been demonstrated that gonadal hormones during puberty can further organize and refine neural circuits^{53,54}. During puberty, pruning and remodeling of synapses, morphology, density, and sexual dimorphism of dendritic spines occurs throughout the brain. In many brain sites, this fine remodeling is orchestrated by gonadal hormones, particularly androgens^{55–59}. Thus, increased *Ar* expression during the prepubertal window in both sexes plays a key role in the continuous developmental process towards the adult brain. Sex differences in circulating steroids during pubertal transition would ultimately determine the circuitry, morphology, and neurochemical fate of the subpopulations of neurons.

Sex differences in *Ar* expression are most apparent in areas related to male sexual behavior and reproduction, including the well characterized BSTpr, MPO, MEApd, and LS^{26,35,60,61}. However, during development, *Ar* expression was similar at PND 12 between males and females in those sites, but apparently higher in males at PND 21, in agreement with previous reports showing greater hypothalamic AR-ir in prepubertal male mice²⁶. Specifically, we found higher *Ar* expression in the SCH of PND 21 males. In adults, SCH AR expression is key for circadian regulation and sex differences in locomotor activity. Orchidectomy feminizes night patterns of activity in males, and androgen replacement restores male-specific patterns of activity^{62,63}. Our findings suggest these differences are established during pubertal development around PND 21. The role of *Esr2* and co-expression with *Ar* is not yet known.

Although at lower levels, *Ar* is still prevalent in the female brain and is expressed in a multitude of different brain nuclei. The role that AR plays in the prepubertal and adult female brain is not fully understood, but models of female androgen excess demonstrate that prenatal and prepubertal androgen exposure has the potential to heavily impact female physiology. For example, polycystic ovary syndrome (PCOS) is partly characterized by female androgen excess, and can significantly impact fertility, body weight and insulin sensitivity^{64–66}. PCOS-like features can be replicated in mice, with one prepubertal model inducing androgen excess beginning at PND 19⁶⁷ and another at PND 21⁶⁸. This peripubertal androgenization model induces changes upon multiple tissues, including the brain, eliciting well described effects on reproduction and metabolism^{69,70}. The exact brain sites associated with the consequences of hyperandrogenism in females have not been fully determined. Defining selective and non-selective brain sites responsive to androgens is an important first step for a better mechanistic understanding of the pathological origins of diseases of androgen excess.

Brain AR expression and distribution have been previously characterized in the rat^{61,71}, hamster⁷², musk shrew⁷³, and monkey⁷⁴. These findings, however, are not directly translatable to the mouse due to species differences. For example, AR is abundant in the dorsomedial VMH (VMHdm) of adult male rats^{20,61,71}, but much less so in adult male

mice. A direct comparative analysis will be necessary, but the VMHdm is highly associated with glucose homeostasis and metabolic control in mice^{75,76}. Whether AR in VMHdm neurons has similar metabolic effects in the mouse versus rat requires further investigation. It is important to be aware of species differences, particularly in the mouse, which is a frequently used model organism in studies using genetic and molecular tools. Furthermore, because the number of neurons necessary for a specific function may not be determined *a priori*, moderate and low AR expression in extra-hypothalamic and extra-limbic areas is not irrelevant or less important. Consistent with this concept, *Ar* expression in cranial nerve nuclei of both sexes during pre-pubertal development is particularly interesting. Many nuclei along the olfactory and auditory pathways express AR, but studies exploring the role of androgenic signaling in cranial nerve nuclei have been limited^{77,78}. Androgens promote neuronal survival and axon regeneration in cranial nerve motor nuclei in male and female rats^{79,80}. In the spinal cord, however, androgens acting on AR protect against motor neuron death in the spinal nucleus of the bulbocavernosus (SNB) during postnatal development in males, resulting in a male-biased sex difference in cell number and morphology^{81,82}. It remains to be determined as to why circulating androgens induce sexual dimorphism in some areas of the brain, but not others, and why specific cell populations respond to androgens, rather than estrogens, to promote neuronal survival, and if these events occur before puberty when androgens are low but AR expression is present in many nuclei of both sexes. Answers to these questions may require a closer look into the regulation of AR signaling complexity, including the role of alternative ligands and ligand-independent signaling properties⁸³.

While this study examines the distribution of AR in male and female prepubertal mice, we have not systemically mapped estrogen receptors in the same experimental groups. Instead, we have examined the expression of two estrogen receptors (ER α / β) in select nuclei which express *Ar* during development. It is highly possible however, that subpopulations of cells in these areas only transiently express AR, ER α and/or ER β during development as observed in the forebrain^{84,85}. Furthermore, AR and ERs can interact with each other to modulate transactivation or signaling activity⁸⁶. For example, ER β can down-regulate AR in the ventral prostate⁸⁷, while AR can either inhibit or support ER α activity in breast cancer cells^{88,89}. Additional studies will be necessary to define specific time points of prepubertal development in which subpopulations of neurons are engaged by selective gonadal steroids, and the interaction of different steroid receptor pathways.

Gonadal hormones are not the only factor that contribute to sex differences in the brain. Sex chromosome genes, autosome genes whose expression are mediated by sex-steroid receptors, epigenetics, environmental factors and exposures, factors which regulate the sensitivity of a brain region to sex steroids, and brain immune cells all contribute to brain sex differentiation⁹⁰. Yet, it is clear that androgens play a very important, arguably dominant role in sex differentiation in rodents via AR or ERs, and their unknown role in female brain remains to be fully determined. In the attempt to decrease this gap, we focused our analysis on both sexes. Our findings indicate that in various brain areas androgens, in addition to neuroestrogens or circulating estrogens, may also contribute to female neuronal development and physiology. They also highlight the need for greater investigation into the

variety of actions of androgens throughout the male and female brain, particularly during prepubertal development. Future studies targeting specific brain sites are warranted.

Acknowledgments:

We would like to thank Susan Allen for expert technical assistance. This research was supported by funding from National Institute of Health (NIH) Grants R01HD069702 and R01HD096324 (CFE). AC was supported by NIH T32HD079342.

References

1. Koopman P, Münsterberg A, Capel B, Vivian N, Lovell-Badge R. Expression of a candidate sex-determining gene during mouse testis differentiation. *Nature* 1990;348(6300):450–452. [PubMed: 2247150]
2. Sinclair AH, Berta P, Palmer MS, et al. A gene from the human sex-determining region encodes a protein with homology to a conserved DNA-binding motif. *Nature* 1990;346(6281):240–244. [PubMed: 1695712]
3. Rhoda J, Corbier P, Roffi J. Gonadal Steroid Concentrations in Serum and Hypothalamus of the Rat at Birth: Aromatization of Testosterone to 17 β -Estradiol*. *Endocrinology* 1984;114(5):1754–1760. [PubMed: 6714163]
4. Weisz J, Ward IL. Plasma Testosterone and Progesterone Titters of Pregnant Rats, Their Male and Female Fetuses, and Neonatal Offspring*. *Endocrinology* 1980;106(1):306–316. [PubMed: 7349961]
5. Naftolin F, MacLusky N. Aromatization hypothesis revisited. *Sexual differentiation: Basic and clinical aspects*: Raven Press New York; 1984:79–91.
6. McEwen BS, Lieberburg I, Chaptal C, Krey LC. Aromatization: Important for sexual differentiation of the neonatal rat brain. *Hormones and Behavior* 1977;9(3):249–263. [PubMed: 611076]
7. Naftolin F, Ryan KJ, Davies IJ, et al. The Formation of Estrogens by Central Neuroendocrine Tissues. In: Greep RO, ed. *Proceedings of the 1974 Laurentian Hormone Conference Vol 31*. Boston: Academic Press; 1975:295–319.
8. McCarthy MM, Schlenker EH, Pfaff DW. Enduring consequences of neonatal treatment with antisense oligodeoxynucleotides to estrogen receptor messenger ribonucleic acid on sexual differentiation of rat brain. *Endocrinology* 1993;133(2):433–439. [PubMed: 8344188]
9. Shughrue PJ, Lane MV, Merchenthaler I. Comparative distribution of estrogen receptor- α and - β mRNA in the rat central nervous system. *Journal of Comparative Neurology* 1997;388(4):507–525.
10. Ogawa S, Chan J, Chester AE, Gustafsson J-Å, Korach KS, Pfaff DW. Survival of reproductive behaviors in estrogen receptor β gene-deficient (β ERKO) male and female mice. *Proceedings of the National Academy of Sciences* 1999;96(22):12887–12892.
11. Wersinger SR, Sannen K, Villalba C, Lubahn DB, Rissman EF, De Vries GJ. Masculine Sexual Behavior Is Disrupted in Male and Female Mice Lacking a Functional Estrogen Receptor α Gene. *Hormones and Behavior* 1997;32(3):176–183. [PubMed: 9454668]
12. Arnold AP, Gorski RA. Gonadal Steroid Induction of Structural Sex Differences in the Central Nervous System. *Annual Review of Neuroscience* 1984;7(1):413–442.
13. Arnold AP, Breedlove SM. Organizational and activational effects of sex steroids on brain and behavior: A reanalysis. *Hormones and Behavior* 1985;19(4):469–498. [PubMed: 3910535]
14. Phoenix CH, Goy RW, Gerall AA, Young WC. Organizing action of prenatally administered testosterone propionate on the tissues mediating mating behavior in the female guinea pig I. *Endocrinology* 1959;65(3):369–382. [PubMed: 14432658]
15. Keller M, Pawluski JL, Brock O, Douhard Q, Bakker J. The alpha-fetoprotein knock-out mouse model suggests that parental behavior is sexually differentiated under the influence of prenatal estradiol. *Hormones and behavior* 2010;57(4–5):434–440. [PubMed: 20109458]
16. Vannier B, Raynaud JP. Effect of estrogen plasma binding on sexual differentiation of the rat fetus. *Molecular and cellular endocrinology* 1975;3(5):323–337. [PubMed: 53165]

17. Hines M, Allen LS, Gorski RA. Sex differences in subregions of the medial nucleus of the amygdala and the bed nucleus of the stria terminalis of the rat. *Brain Res* 1992;579(2):321–326. [PubMed: 1352729]
18. Lisciotto CA, Morrell JI. Sex differences in the distribution and projections of testosterone target neurons in the medial preoptic area and the bed nucleus of the stria terminalis of rats. *Horm Behav* 1994;28(4):492–502. [PubMed: 7729818]
19. Madeira MD, Ferreira-Silva L, Paula-Barbosa MM. Influence of sex and estrus cycle on the sexual dimorphisms of the hypothalamic ventromedial nucleus: stereological evaluation and Golgi study. *J Comp Neurol* 2001;432(3):329–345. [PubMed: 11246211]
20. Dugger BN, Morris JA, Jordan CL, Breedlove SM. Androgen receptors are required for full masculinization of the ventromedial hypothalamus (VMH) in rats. *Horm Behav* 2007;51(2):195–201. [PubMed: 17123532]
21. Abreu AP, Kaiser UB. Pubertal development and regulation. *Lancet Diabetes Endocrinol* 2016;4(3):254–264. [PubMed: 26852256]
22. Bakker J, Baum MJ. Role for estradiol in female-typical brain and behavioral sexual differentiation. *Front Neuroendocrinol* 2008;29(1):1–16. [PubMed: 17720235]
23. Nilsson ME, Vandenput L, Tivesten A, et al. Measurement of a Comprehensive Sex Steroid Profile in Rodent Serum by High-Sensitive Gas Chromatography-Tandem Mass Spectrometry. *Endocrinology* 2015;156(7):2492–2502. [PubMed: 25856427]
24. Gupta D, Attanasio A, Raaf S. Plasma Estrogen and Androgen Concentrations in Children During Adolescence. *The Journal of Clinical Endocrinology & Metabolism* 1975;40(4):636–643. [PubMed: 1127074]
25. Kushnir MM, Blamires T, Rockwood AL, et al. Liquid Chromatography–Tandem Mass Spectrometry Assay for Androstenedione, Dehydroepiandrosterone, and Testosterone with Pediatric and Adult Reference Intervals. *Clinical Chemistry* 2010;56(7):1138–1147. [PubMed: 20489135]
26. Brock O, De Mees C, Bakker J. Hypothalamic expression of oestrogen receptor alpha and androgen receptor is sex-, age- and region-dependent in mice. *J Neuroendocrinol* 2015;27(4):264–276. [PubMed: 25599767]
27. Hou H, Uusküla-Reimand L, Makarem M, et al. Gene expression profiling of puberty-associated genes reveals abundant tissue and sex-specific changes across postnatal development. *Human Molecular Genetics* 2017;26(18):3585–3599. [PubMed: 28911201]
28. Han X, Burger LL, Garcia-Galiano D, et al. Hypothalamic and Cell-Specific Transcriptomes Unravel a Dynamic Neuropil Remodeling in Leptin-Induced and Typical Pubertal Transition in Female Mice. *iScience* 2020;23(10):101563. [PubMed: 33083731]
29. Gorski RA. Sexual Differentiation of the Brain. *Hospital Practice* 1978;13(10):55–62. [PubMed: 569631]
30. Tsukahara S, Morishita M. Sexually Dimorphic Formation of the Preoptic Area and the Bed Nucleus of the Stria Terminalis by Neuroestrogens. *Frontiers in Neuroscience* 2020;14(797).
31. Marrocco J, McEwen BS. Sex in the brain: hormones and sex differences. *Dialogues in clinical neuroscience* 2016;18(4):373–383. [PubMed: 28179809]
32. Altemus M, Sarvaiya N, Neill Epperson C. Sex differences in anxiety and depression clinical perspectives. *Front Neuroendocrinol* 2014;35(3):320–330. [PubMed: 24887405]
33. Wood RI, Newman SW. Androgen and Estrogen Receptors Coexist within Individual Neurons in the Brain of the Syrian Hamster. *Neuroendocrinology* 1995;62(5):487–497. [PubMed: 8559280]
34. Jahan MR, Kokubu K, Islam MN, et al. Species differences in androgen receptor expression in the medial preoptic and anterior hypothalamic areas of adult male and female rodents. *Neuroscience* 2015;284:943–961. [PubMed: 25446364]
35. Shah NM, Pisapia DJ, Maniatis S, Mendelsohn MM, Nemes A, Axel R. Visualizing sexual dimorphism in the brain. *Neuron* 2004;43(3):313–319. [PubMed: 15294140]
36. Lu SF, McKenna SE, Cologer-Clifford A, Nau EA, Simon NG. Androgen receptor in mouse brain: sex differences and similarities in autoregulation. *Endocrinology* 1998;139(4):1594–1601. [PubMed: 9528939]

37. Apostolinas S, Rajendren G, Dobrjansky A, Gibson MJ. Androgen receptor immunoreactivity in specific neural regions in normal and hypogonadal male mice: effect of androgens. *Brain Res* 1999;817(1–2):19–24. [PubMed: 9889303]
38. Council NR. Guide for the Care and Use of Laboratory Animals: Eighth Edition Washington, DC: The National Academies Press; 2011.
39. Oyegbile TO, Marler CA. Winning fights elevates testosterone levels in California mice and enhances future ability to win fights. *Hormones and Behavior* 2005;48(3):259–267. [PubMed: 15979073]
40. Caligioni C. Assessing Reproductive Status/Stages in Mice. *Current protocols in neuroscience / editorial board, Jacqueline N Crawley [et al]* 2009:Appendix-4I.
41. Silveira MA, Wagenmaker ER, Burger LL, DeFazio RA, Moenter SM. GnRH Neuron Activity and Pituitary Response in Estradiol-Induced vs Proestrous Luteinizing Hormone Surges in Female Mice. *Endocrinology* 2016;158(2):356–366.
42. Low KL, Ma C, Soma KK. Tyramide Signal Amplification Permits Immunohistochemical Analyses of Androgen Receptors in the Rat Prefrontal Cortex. *J Histochem Cytochem* 2017;65(5):295–308. [PubMed: 28438093]
43. Paxinos G, Franklin KBJ. Paxinos and Franklin's the mouse brain in stereotaxic coordinates : George Paxinos, Keith B.J. Franklin 2019.
44. Rodrigues BC, Cavalcante JC, Elias CF. Expression of cocaine- and amphetamine-regulated transcript in the rat forebrain during postnatal development. *Neuroscience* 2011;195:201–214. [PubMed: 21903152]
45. Cavalcante JC, Bittencourt JC, Elias CF. Female odors stimulate CART neurons in the ventral premammillary nucleus of male rats. *Physiology & Behavior* 2006;88(1):160–166. [PubMed: 16687159]
46. Rissman EF, Wersinger SR, Taylor JA, Lubahn DB. Estrogen Receptor Function as Revealed by Knockout Studies: Neuroendocrine and Behavioral Aspects. *Hormones and Behavior* 1997;31(3):232–243. [PubMed: 9213137]
47. Ogawa S, Chester AE, Hewitt SC, et al. Abolition of male sexual behaviors in mice lacking estrogen receptors alpha and beta (alpha beta ERKO). *Proceedings of the National Academy of Sciences of the United States of America* 2000;97(26):14737–14741. [PubMed: 11114183]
48. Wu MV, Manoli DS, Fraser EJ, et al. Estrogen masculinizes neural pathways and sex-specific behaviors. *Cell* 2009;139(1):61–72. [PubMed: 19804754]
49. Mayer C, Acosta-Martinez M, Dubois SL, et al. Timing and completion of puberty in female mice depend on estrogen receptor α -signaling in kisspeptin neurons. *Proceedings of the National Academy of Sciences* 2010;107(52):22693–22698.
50. Merchenthaler I, Lane MV, Numan S, Dellovade TL. Distribution of estrogen receptor α and β in the mouse central nervous system: In vivo autoradiographic and immunocytochemical analyses. *Journal of Comparative Neurology* 2004;473(2):270–291.
51. Saito K, He Y, Yan X, et al. Visualizing estrogen receptor- α -expressing neurons using a new ER α -ZsGreen reporter mouse line. *Metabolism* 2016;65(4):522–532. [PubMed: 26975544]
52. Lubahn DB, Moyer JS, Golding TS, Couse JF, Korach KS, Smithies O. Alteration of reproductive function but not prenatal sexual development after insertional disruption of the mouse estrogen receptor gene. *Proceedings of the National Academy of Sciences of the United States of America* 1993;90(23):11162–11166. [PubMed: 8248223]
53. Sisk CL, Zehr JL. Pubertal hormones organize the adolescent brain and behavior. *Front Neuroendocrinol* 2005;26(3–4):163–174. [PubMed: 16309736]
54. Schulz KM, Zehr JL, Salas-Ramirez KY, Sisk CL. Testosterone programs adult social behavior before and during, but not after, adolescence. *Endocrinology* 2009;150(8):3690–3698. [PubMed: 19423759]
55. Frankfurt M, Gould E, Woolley CS, McEwen BS. Gonadal steroids modify dendritic spine density in ventromedial hypothalamic neurons: a Golgi study in the adult rat. *Neuroendocrinology* 1990;51(5):530–535. [PubMed: 2112730]

56. Gould E, Woolley CS, Frankfurt M, McEwen BS. Gonadal steroids regulate dendritic spine density in hippocampal pyramidal cells in adulthood. *J Neurosci* 1990;10(4):1286–1291. [PubMed: 2329377]
57. Hatanaka Y, Hojo Y, Mukai H, et al. Rapid increase of spines by dihydrotestosterone and testosterone in hippocampal neurons: Dependence on synaptic androgen receptor and kinase networks. *Brain Res* 2015;1621:121–132. [PubMed: 25511993]
58. Leranth C, Petnehazy O, MacLusky NJ. Gonadal Hormones Affect Spine Synaptic Density in the CA1 Hippocampal Subfield of Male Rats. *The Journal of Neuroscience* 2003;23(5):1588–1592. [PubMed: 12629162]
59. Leranth C, Hajszan T, MacLusky NJ. Androgens Increase Spine Synapse Density in the CA1 Hippocampal Subfield of Ovariectomized Female Rats. *The Journal of Neuroscience* 2004;24(2):495–499. [PubMed: 14724248]
60. Juntti SA, Tollkuhn J, Wu MV, et al. The androgen receptor governs the execution, but not programming, of male sexual and territorial behaviors. *Neuron* 2010;66(2):260–272. [PubMed: 20435002]
61. McAbee MD, DonCarlos LL. Ontogeny of region-specific sex differences in androgen receptor messenger ribonucleic acid expression in the rat forebrain. *Endocrinology* 1998;139(4):1738–1745. [PubMed: 9528957]
62. Iwahana E, Karatsoreos I, Shibata S, Silver R. Gonadectomy reveals sex differences in circadian rhythms and suprachiasmatic nucleus androgen receptors in mice. *Hormones and Behavior* 2008;53(3):422–430. [PubMed: 18164002]
63. Karatsoreos IN, Wang A, Sasanian J, Silver R. A Role for Androgens in Regulating Circadian Behavior and the Suprachiasmatic Nucleus. *Endocrinology* 2007;148(11):5487–5495. [PubMed: 17702841]
64. Huang A, Brennan K, Azziz R. Prevalence of hyperandrogenemia in the polycystic ovary syndrome diagnosed by the National Institutes of Health 1990 criteria. *Fertility and sterility* 2010;93(6):1938–1941. [PubMed: 19249030]
65. Sanchez-Garrido MA, Tena-Sempere M. Metabolic dysfunction in polycystic ovary syndrome: Pathogenic role of androgen excess and potential therapeutic strategies. *Mol Metab* 2020;35:100937. [PubMed: 32244180]
66. Dumesic DA, Oberfield SE, Stener-Victorin E, Marshall JC, Laven JS, Legro RS. Scientific Statement on the Diagnostic Criteria, Epidemiology, Pathophysiology, and Molecular Genetics of Polycystic Ovary Syndrome. *Endocr Rev* 2015;36(5):487–525. [PubMed: 26426951]
67. van Houten EL, Kramer P, McLuskey A, Karels B, Themmen AP, Visser JA. Reproductive and metabolic phenotype of a mouse model of PCOS. *Endocrinology* 2012;153(6):2861–2869. [PubMed: 22334715]
68. Caldwell AS, Middleton LJ, Jimenez M, et al. Characterization of reproductive, metabolic, and endocrine features of polycystic ovary syndrome in female hyperandrogenic mouse models. *Endocrinology* 2014;155(8):3146–3159. [PubMed: 24877633]
69. Aflatoonian A, Edwards MC, Rodriguez Paris V, et al. Androgen signaling pathways driving reproductive and metabolic phenotypes in a PCOS mouse model. *The Journal of endocrinology* 2020;245(3):381–395. [PubMed: 32229702]
70. Caldwell ASL, Edwards MC, Desai R, et al. Neuroendocrine androgen action is a key extraovarian mediator in the development of polycystic ovary syndrome. *Proceedings of the National Academy of Sciences of the United States of America* 2017;114(16):E3334–E3343. [PubMed: 28320971]
71. Simerly RB, Chang C, Muramatsu M, Swanson LW. Distribution of androgen and estrogen receptor mRNA-containing cells in the rat brain: an in situ hybridization study. *J Comp Neurol* 1990;294(1):76–95. [PubMed: 2324335]
72. Wood RI, Newman SW. Androgen receptor immunoreactivity in the male and female Syrian hamster brain. *J Neurobiol* 1999;39(3):359–370. [PubMed: 10363909]
73. Veney SL, Rissman EF. Immunolocalization of androgen receptors and aromatase enzyme in the adult musk shrew brain. *Neuroendocrinology* 2000;72(1):29–36. [PubMed: 10940736]

74. Roselli CE, Klosterman S, Resko JA. Anatomic relationships between aromatase and androgen receptor mRNA expression in the hypothalamus and amygdala of adult male cynomolgus monkeys. *J Comp Neurol* 2001;439(2):208–223. [PubMed: 11596049]
75. Flak JN, Goforth PB, Dell’Orco J, et al. Ventromedial hypothalamic nucleus neuronal subset regulates blood glucose independently of insulin. *The Journal of clinical investigation* 2020;130(6):2943–2952. [PubMed: 32134398]
76. Castorena CM, Caron A, Michael NJ, et al. CB1Rs in VMH neurons regulate glucose homeostasis but not body weight. *American journal of physiology Endocrinology and metabolism* 2021;321(1):E146–e155. [PubMed: 34097543]
77. Yu WH, McGinnis MY. Androgen receptors in cranial nerve motor nuclei of male and female rats. *J Neurobiol* 2001;46(1):1–10. [PubMed: 11108611]
78. Sar M, Stumpf W. Androgen concentration in motor neurons of cranial nerves and spinal cord. *Science* 1977;197(4298):77–79. [PubMed: 867053]
79. Yu WH. Administration of testosterone attenuates neuronal loss following axotomy in the brain-stem motor nuclei of female rats. *J Neurosci* 1989;9(11):3908–3914. [PubMed: 2585059]
80. Amy Yu W-h. Effect of testosterone on the regeneration of the hypoglossal nerve in rats. *Experimental Neurology* 1982;77(1):129–141. [PubMed: 7084387]
81. Nordeen E, Nordeen K, Sengelaub D, Arnold A. Androgens prevent normally occurring cell death in a sexually dimorphic spinal nucleus. *Science* 1985;229(4714):671–673. [PubMed: 4023706]
82. Breedlove SM, Arnold AP. Sexually dimorphic motor nucleus in the rat lumbar spinal cord: response to adult hormone manipulation, absence in androgen-insensitive rats. *Brain Res* 1981;225(2):297–307. [PubMed: 7306791]
83. Davey RA, Grossmann M. Androgen Receptor Structure, Function and Biology: From Bench to Bedside. *Clin Biochem Rev* 2016;37(1):3–15. [PubMed: 27057074]
84. Zuloaga DG, Zuloaga KL, Hinds LR, Carbone DL, Handa RJ. Estrogen receptor β expression in the mouse forebrain: Age and sex differences. *Journal of Comparative Neurology* 2014;522(2):358–371.
85. Sugiyama N, Andersson S, Lathe R, et al. Spatiotemporal dynamics of the expression of estrogen receptors in the postnatal mouse brain. *Molecular Psychiatry* 2009;14(2):223–232. [PubMed: 18982005]
86. Panet-Raymond V, Gottlieb B, Beitel LK, Pinsky L, Trifiro MA. Interactions between androgen and estrogen receptors and the effects on their transactivational properties. *Molecular and cellular endocrinology* 2000;167(1–2):139–150. [PubMed: 11000528]
87. Wu W-f, Maneix L, Insunza J, et al. Estrogen receptor β , a regulator of androgen receptor signaling in the mouse ventral prostate. *Proceedings of the National Academy of Sciences* 2017;114(19):E3816–E3822.
88. Peters AA, Buchanan G, Ricciardelli C, et al. Androgen receptor inhibits estrogen receptor- α activity and is prognostic in breast cancer. *Cancer research* 2009;69(15):6131–6140. [PubMed: 19638585]
89. D’Amato NC, Gordon MA, Babbs B, et al. Cooperative Dynamics of AR and ER Activity in Breast Cancer. *Molecular cancer research : MCR* 2016;14(11):1054–1067. [PubMed: 27565181]
90. McCarthy MM, Arnold AP. Reframing sexual differentiation of the brain. *Nature Neuroscience* 2011;14(6):677–683. [PubMed: 21613996]

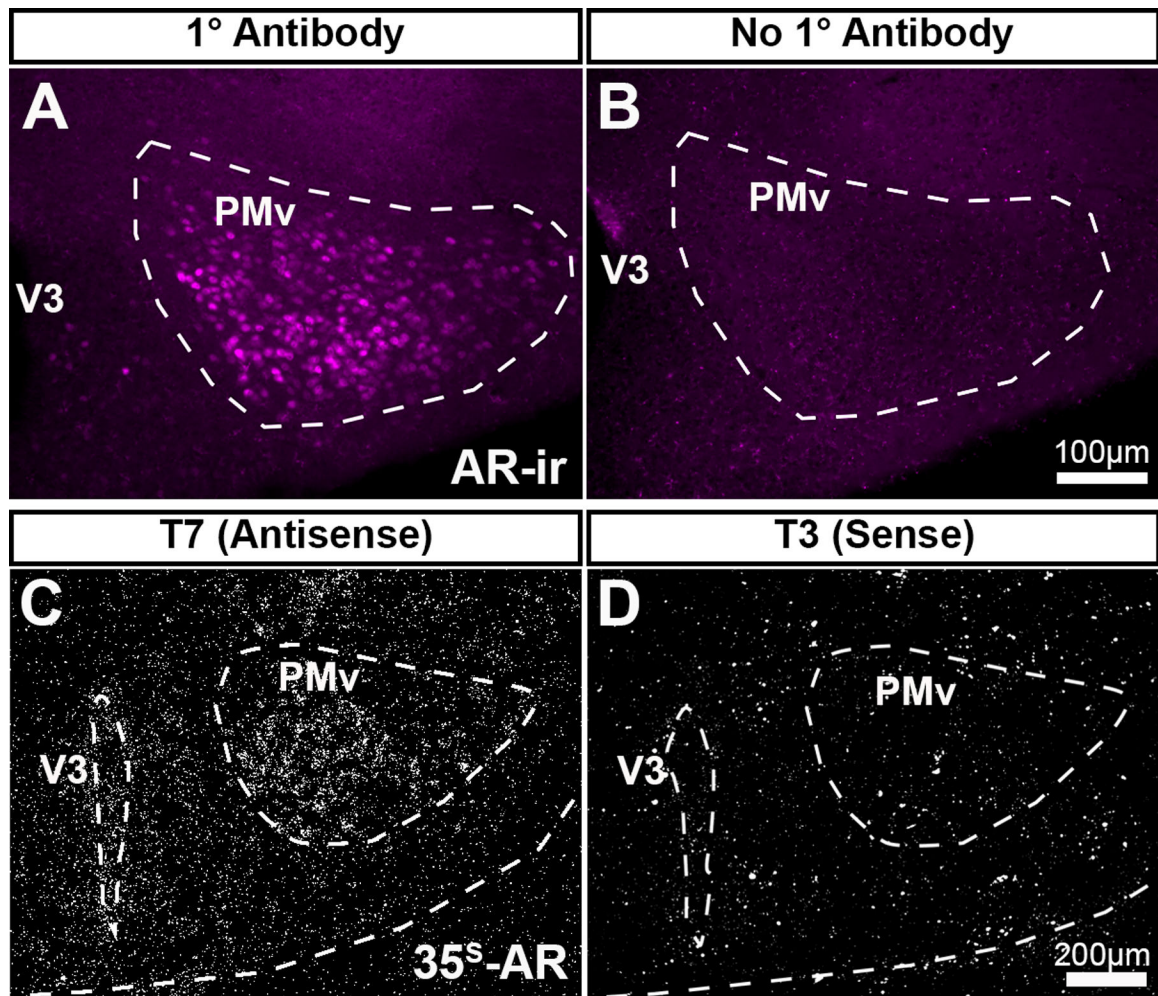


Figure 1: Validation of AR immunohistochemistry and *Ar* *in situ* hybridization probe. A-B, fluorescent images showing AR-immunoreactivity (AR-ir) in the adult female mouse brain (postnatal day/PND 56–70). AR-ir was observed in sections incubated in primary antibody (A), but not in sections without primary antibody (B). C-D, darkfield images showing silver grain deposition corresponding to *Ar* hybridization signal in adjacent sections from the same brain (PND 12 male mouse). Signal was observed in sections hybridized with an antisense probe (C), but not with a sense probe (D). Abbreviations: V3, third ventricle, PMv, ventral premammillary nucleus. Scale bar = 100 µm (A-B), 200 µm (C-D).

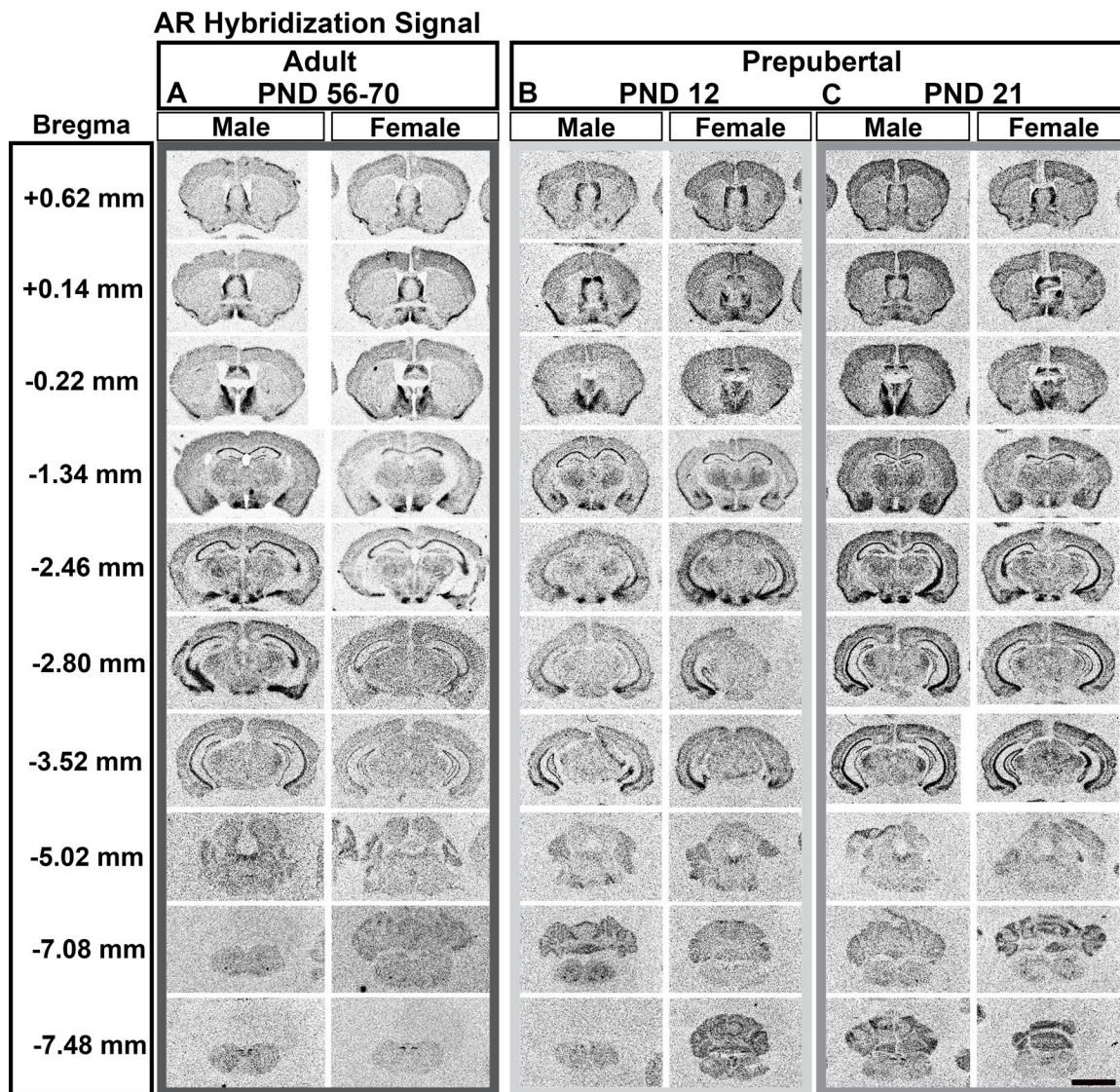


Figure 2: *Ar* mRNA hybridization signal expression in male and female prepubertal and adult brain.
 Images from scanned autoradiographic film of adult (postnatal day/PND 56–70, A), and prepubertal (PND 12, B, and PND 21, C) male and female mouse brain. Select coronal sections are shown in rostral to caudal order. Darker signal indicates higher expression of *Ar* mRNA. Approximate distance from bregma (left column) derived from adult mouse brain (Paxinos and Franklin atlas). Scale bar = 4000 μ m.

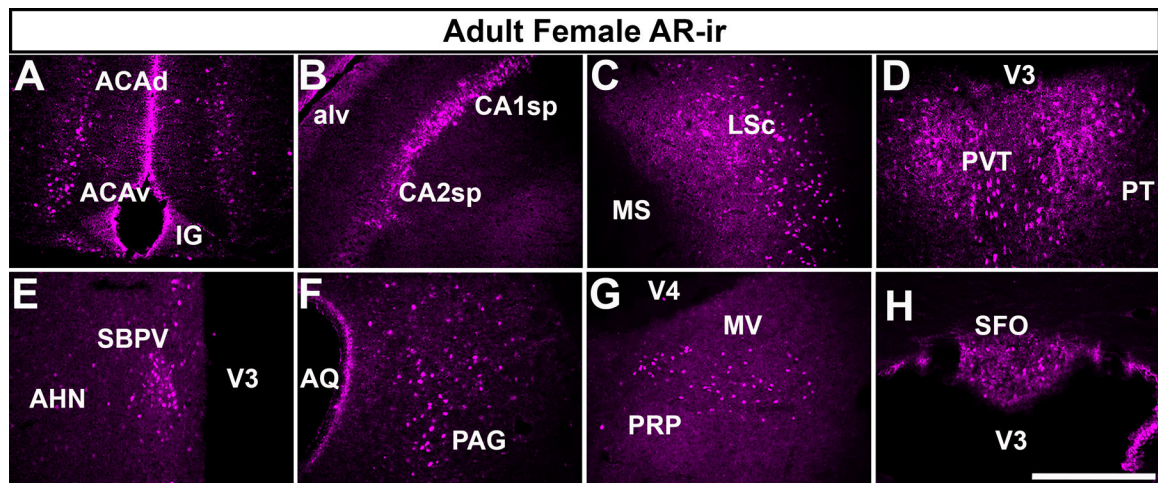


Figure 3: AR immunoreactivity (AR-ir) in adult mouse brain.

A-H, fluorescent images showing AR-ir in the adult female mouse brain (postnatal day/PND 56–70). AR-ir was observed in virtually all areas where we observed *Ar* mRNA. Selected areas from (A) cerebral cortex (dorsal and ventral anterior cingulate area, ACA_d, ACA_v), (B) hippocampal formation (pyramidal layer or sp field CA1 and CA2), (C) cerebral nuclei (lateral septal nucleus, caudodorsal, LSc), (D) thalamus (paraventricular nucleus of the thalamus, PVT), (E) hypothalamus (subparaventricular zone, SBPV), (F) midbrain (periaqueductal gray, PAG), (G) pons/medulla (medial vestibular nucleus, MV), and (H) circumventricular organs (subfornical organ, SFO) are shown. Abbreviations: AHN, anterior hypothalamic nucleus, alv, alveus, AQ, cerebral aqueduct, IG, induseum griseum, MS, medial septal nucleus, PRP, nucleus prepositus, PT, parataenial nucleus, V3, third ventricle, V4, fourth ventricle. Scale bar = 100 μm.

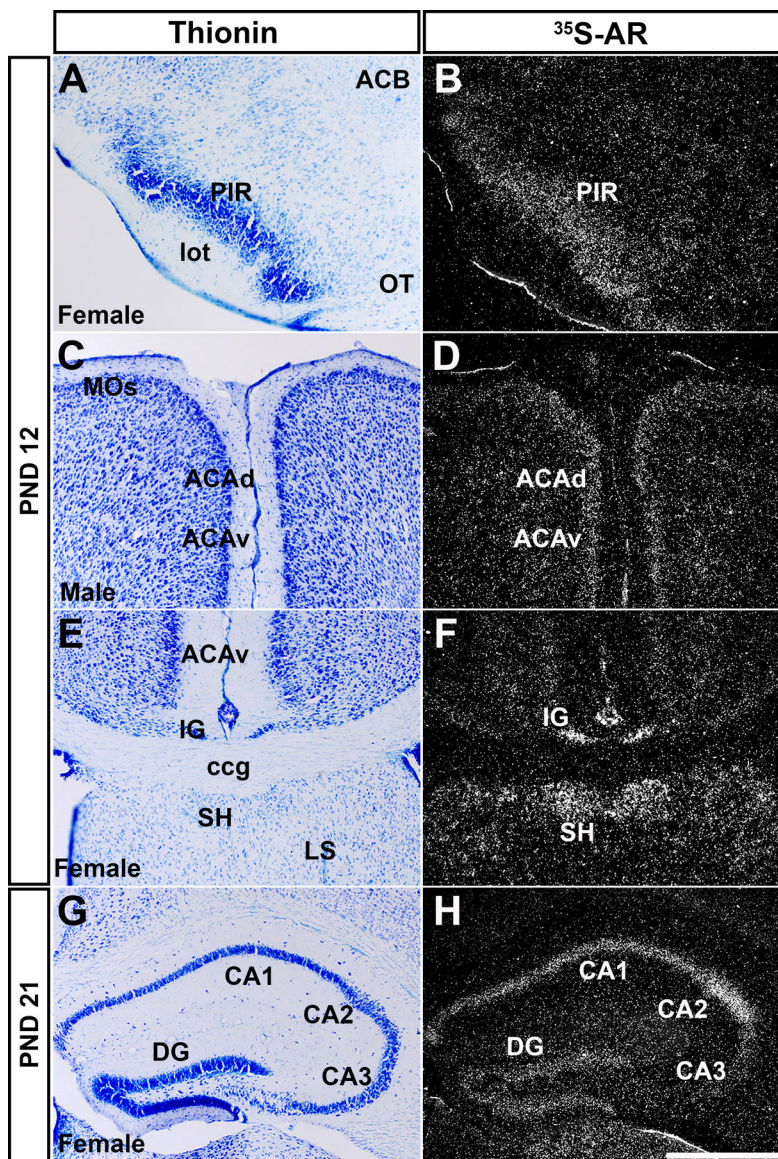


Figure 4: *Ar* mRNA expression in cerebral cortex in prepubertal male and female mice. Images showing thionin staining for neuroanatomical reference (left column), silver grains corresponding to *Ar* mRNA (right column). Low *Ar* expression was observed in the piriform area (PIR, A-B), dorsal and ventral anterior cingulate area (ACAAd and ACAv, C-D), induseum griseum, septohippocampal nucleus (IG and SH, E-F), and CA3, and high in field CA1 and CA2 (G-H). Abbreviations: ACB, nucleus accumbens, ccg, genu of corpus callosum, DG, dentate gyrus, lot, lateral olfactory tract, LS, lateral septal nucleus, MOs, secondary motor area, OT, olfactory tubercle. Scale bar = 200 μ m.

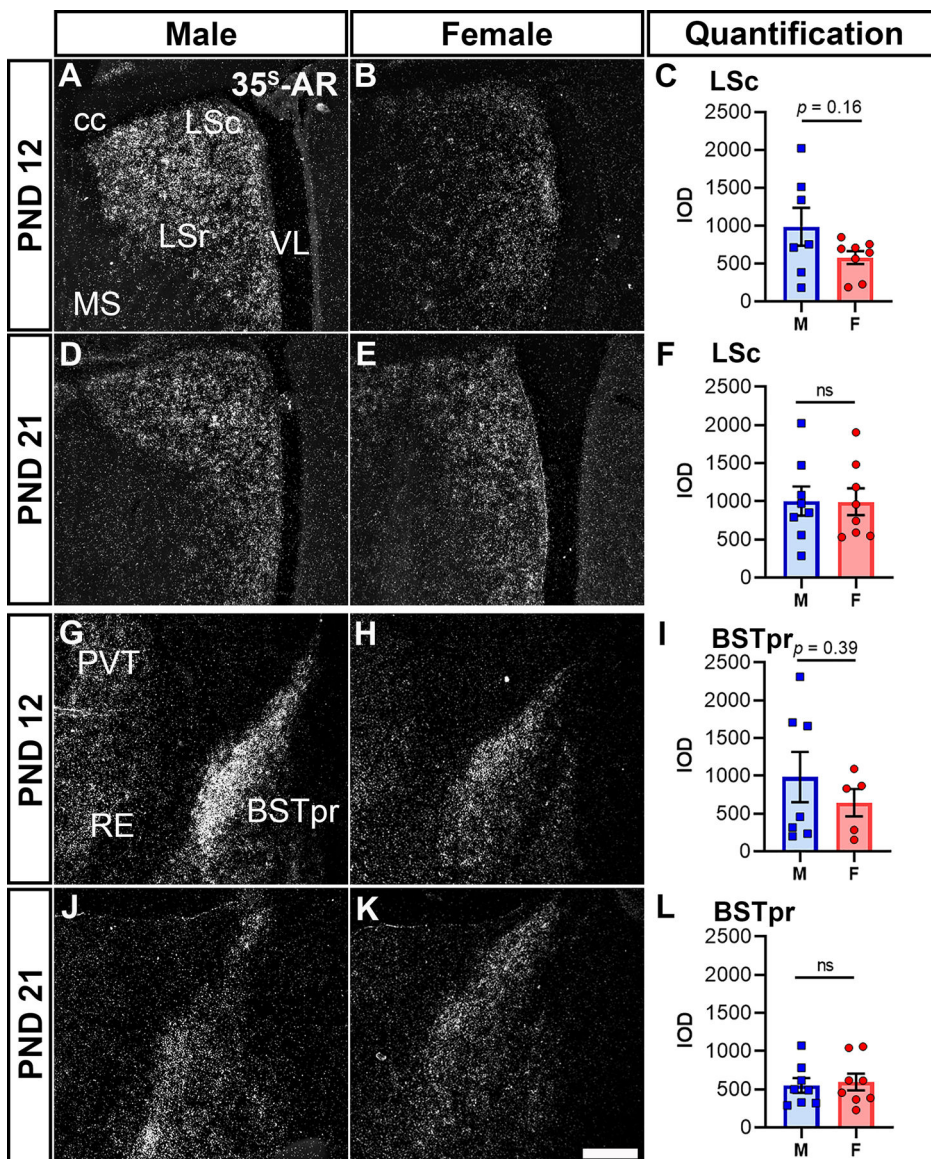


Figure 5: *Ar* mRNA expression in cerebral nuclei of male and female prepubertal mice. Silver grain deposition corresponding to *Ar* mRNA hybridization signal in prepubertal (postnatal day (PND) 12 (A-B, G-H), and PND 21 (D-E, J-K) male (A, D, G, J) and female (B, E, H, K) mice. (A-F) Lateral septal nucleus, caudodorsal (LSc) and (G-L) bed nucleus of the stria terminalis, principal nucleus (BSTpr). Bar graphs showing mean \pm SEM integrated optical density (IOD) of silver grains (C, F, I, L). IOD was analyzed by *t*-test with Welch's correction for LSc male vs female PND 12 ($P = 0.16$, $n = 7-8/\text{sex}$), PND 21 ($P = 0.96$, $n = 8/\text{sex}$), BST male vs female PND 12 ($P = 0.39$, $n = 5-7/\text{sex}$), and BST male vs female PND 21 ($P = 0.75$, $n = 8/\text{sex}$). Abbreviations: cc, corpus callosum, LSr, lateral septal nucleus, rostral (rostroventral), MS, medial septal nucleus, PVT, paraventricular nucleus of the thalamus, RE, nucleus of reuniens, VL, lateral ventricle. Scale bar = 200 μm .

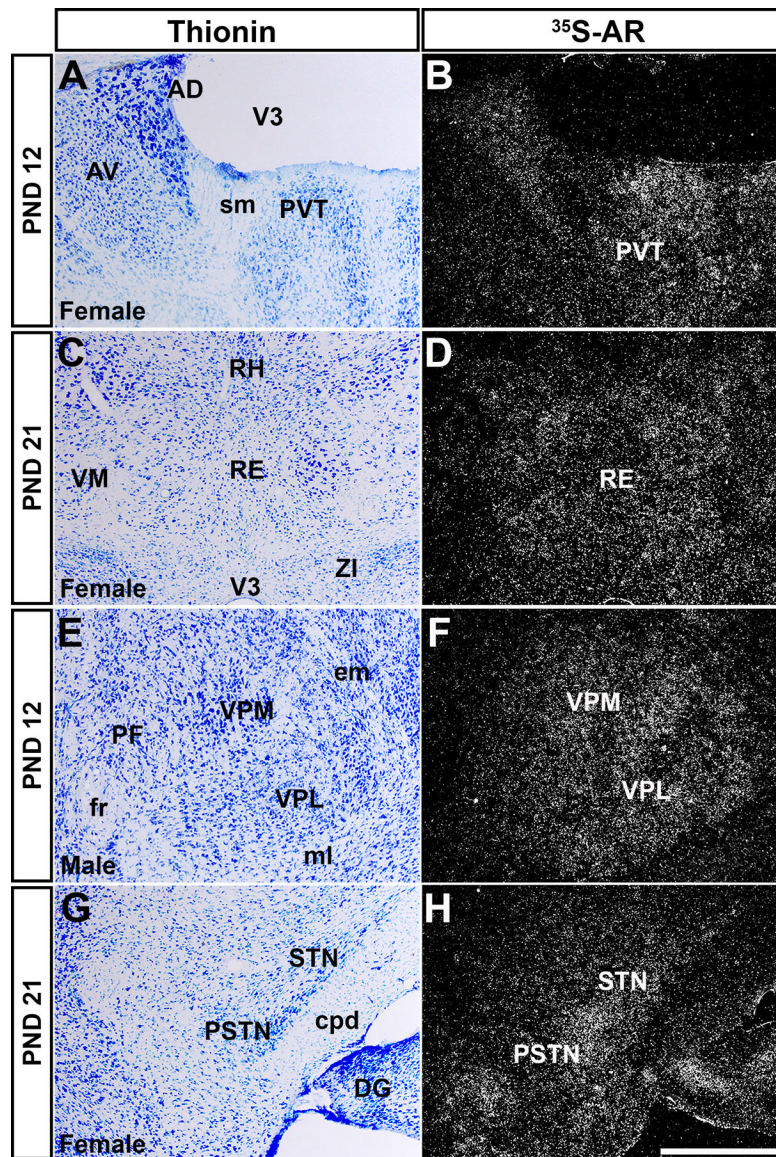


Figure 6: *Ar* mRNA expression in thalamic nuclei of male and female prepubertal mice. Images showing thionin staining for neuroanatomical reference (left column), silver grains corresponding to *Ar* mRNA (right column). (A-B) Low silver grain deposition in the paraventricular nucleus of the thalamus (PVT), (C-D) low to moderate in the nucleus of reuniens (RE), (E-F) ventral posterolateral and posteromedial nuclei of the thalamus (VPL and VPM), (G-H) subthalamic and parasubthalamic nuclei (STN and PSTN). Abbreviations: AD, anterodorsal nucleus of the thalamus, AV, anteroventral nucleus of the thalamus, cpd, cerebral peduncle, DG, dentate gyrus, em, external medullary lamina of the thalamus, fr, fasciculus retroflexus, ml, medial lemniscus, PF, parafascicular nucleus, RH, rhomboid nucleus, sm, stria medullaris, VM, ventral medial nucleus of the thalamus, ZI, zona incerta. Scale bar = 200 μ m.

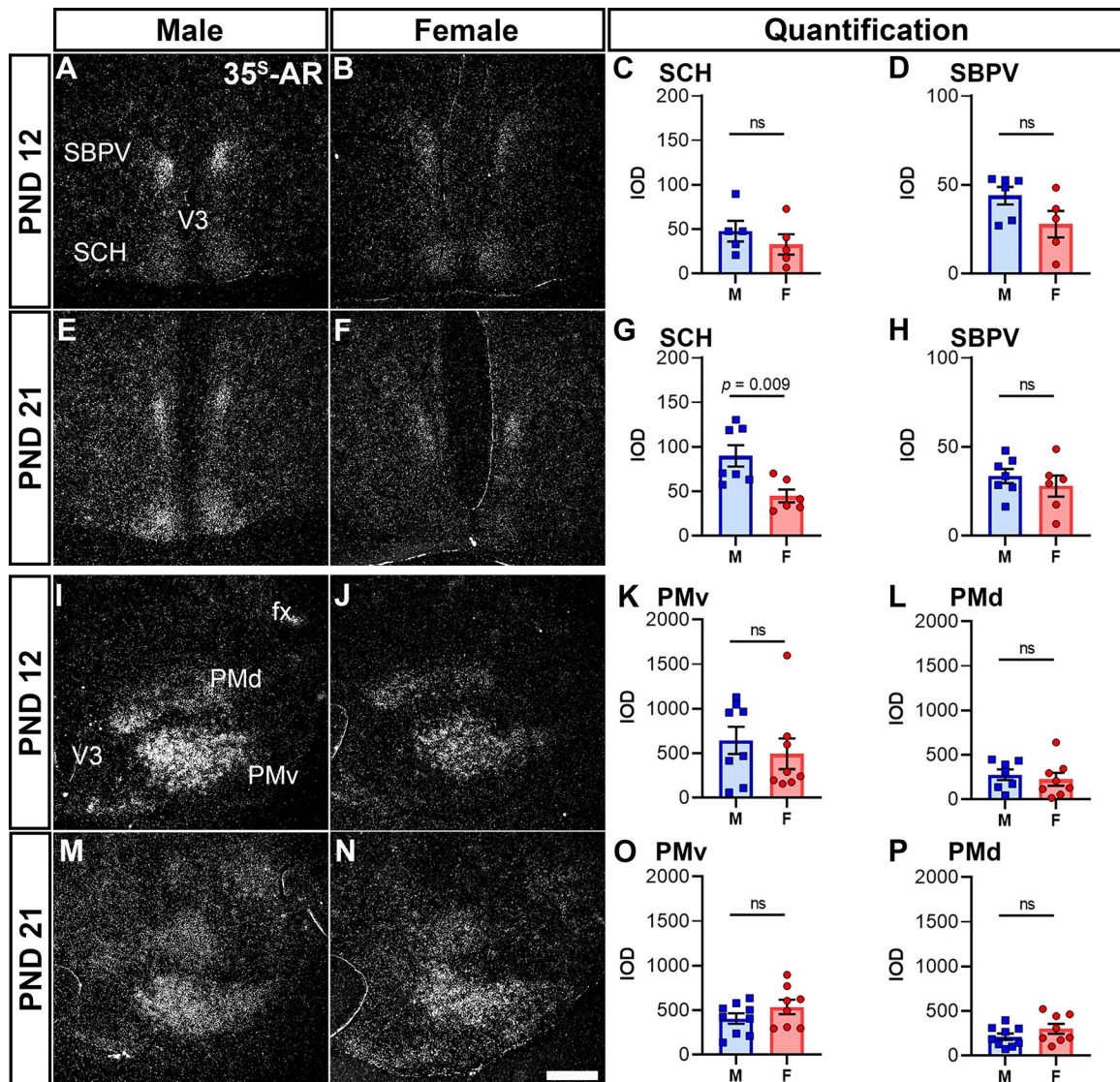


Figure 7: *Ar* mRNA expression in hypothalamic nuclei of male and female prepubertal mice. Silver grain deposition corresponding to *Ar* mRNA hybridization signal in prepubertal (postnatal day (PND) 12 (A-B, I-J), and PND 21 (E-F, M-N) male (A, E, I, M) and female (B, F, J, N) mice. (A-H) Suprachiasmatic nucleus (SCH) and subparaventricular zone (SBPV), and (I-P) dorsal and ventral preammillary nuclei (PMd and PMv). Note higher expression of *Ar* in the SCH of males at PND 21 (E). Bar graphs showing mean \pm SEM integrated optical density (IOD) of silver grains (C-D, G-H, K-L, O-P). IOD was analyzed by *t*-test with Welch's correction for SCH male vs female PND 12 ($P = 0.38$, $n = 5/\text{sex}$), SCH male vs female PND 21 ($P = 0.009$, $n = 6-7/\text{sex}$), SBPV male vs female PND 21 ($P = 0.45$, $n = 6-7/\text{sex}$), PMv male vs female PND 21 ($P = 0.21$, $n = 8-9/\text{sex}$), PMd male vs female PND 12 ($P = 0.58$, $n = 7-8/\text{sex}$) and PND 21 ($P = 0.19$, $n = 8-9/\text{sex}$), and Mann-Whitney nonparametric test for SBPV male vs female PND 12 ($P = 0.12$, $n = 6/\text{sex}$), and PMv male vs female PND 12 ($P = 0.57$, $n = 8/\text{sex}$) Abbreviations: fx, fornix, V3, third ventricle. Scale bar = 200 μm .

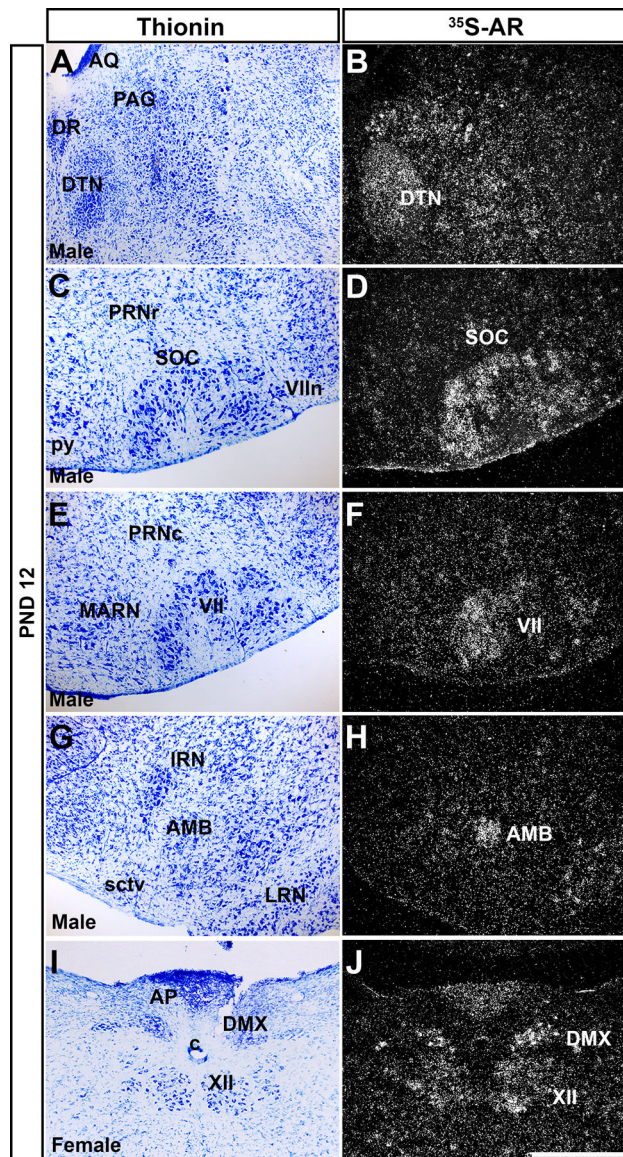


Figure 8: *Ar* mRNA expression in brainstem nuclei of prepubertal male and female mice. Images showing thionin staining for neuroanatomical reference (left column), silver grains corresponding to *Ar* mRNA (right column). (A-B) Very low to low silver grain deposition in the periaqueductal gray (PAG), and low in the dorsal tegmental nucleus (DTN). (C-D) Low expression in the superior olivary complex (SOC), (E-F) facial motor nucleus (VII). (G-H) Moderate expression in the nucleus ambiguus (AMB). (I-J) Low to moderate expression in the dorsal motor nucleus of the vagus nerve (DMX) and hypoglossal nucleus (XII). Abbreviations: VIIIn, facial nerve, AP, area postrema, AQ, cerebral aqueduct, c, central canal of the spinal cord/medulla, DR, dorsal nucleus raphe, IRN, intermediate reticular nucleus, LRN, lateral reticular nucleus, MARN, magnocellular reticular nucleus, PRNc, pontine reticular nucleus, caudal part, PRNr, pontine reticular nucleus, py, pyramid, sctv, ventral spinocerebellar tract. Scale bar = 200 μ m.

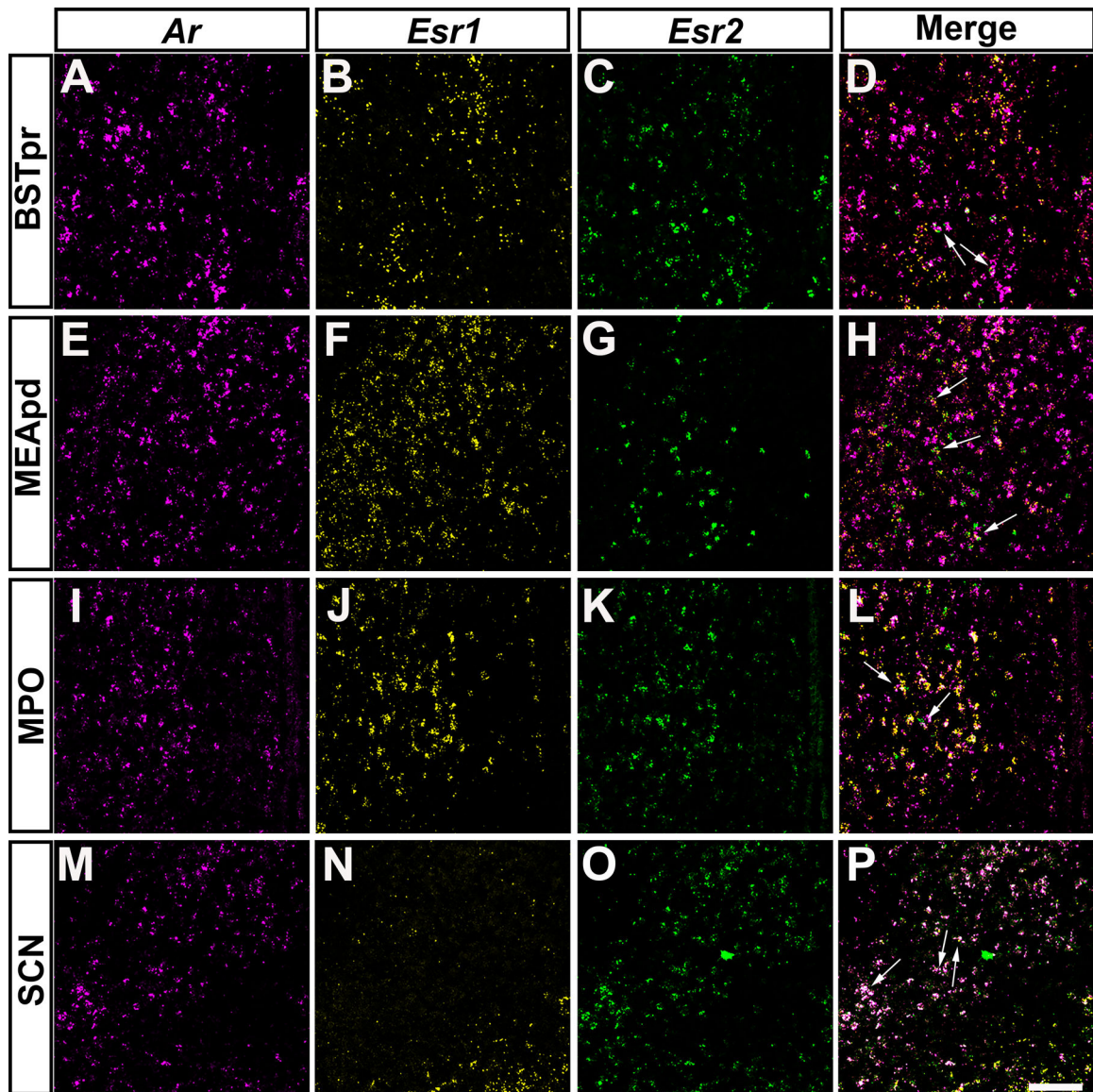


Figure 9: *Ar* mRNA expression overlaps with *Esr1* and *Esr2* in specific forebrain nuclei of prepubertal mice.

A-P, images showing fluorescent *in situ* hybridization signal for *Ar* (magenta, A, E, I, M), *Esr1* (yellow, B, F, J, N), and *Esr2* (green, C, G, K, O). Merge of all 3 channels shown in D, H, L, and P. Areas with *Ar* and *Esr1* and/or *Esr2* co-expression include the bed nucleus of the stria terminalis, principal nucleus (BSTpr, A-D), medial amygdalar nucleus, posterodorsal (MEApd, E-H), medial preoptic area (MPO, I-L), suprachiasmatic nucleus (SCH, M-P). Arrows show dual or triple-labeled neurons. Images shown are from postnatal day 12 (PND 12) female (BSTpr, MEApd, MPO) and male (SCH) mice. Scale bar = 100 μ m.

Table 1:
Qualitative expression of *Ar* mRNA distribution by nuclei in postnatal and adult mouse brain.

–, +/-, +, ++, +++, and ++++ represent not detected, very low, low, moderate, high, and very high expression of silver grain deposits corresponding to *Ar* mRNA. The Allen Mouse Brain Atlas was used as a reference for names, abbreviations, and location of nuclei.

Brain areas and nuclei	Adult		Prepubertal			
	PND 56–70		PND 12		PND 21	
	Male	Female	Male	Female	Male	Female
Cerebral Cortex						
Motor (MO)	+/-	+/-	+/-	+/-	+/-	+/-
Olfactory nucleus (Anterior) (AON)	-	-	++	++	++	++
Taenia tecta (TT)	+	+/-	+	+	+	+
Piriform (PIR)	+	+	+	+	+	+
Cingulate (Anterior) (ACA)	+	+	+	+	+	+
Endopiriform (EP)	+/-	+/-	+/-	+/-	+	+/-
Hippocampal Formation						
Induseum griseum (IG)	+	+	+	+	+	+
Field CA1 (CA1)	+++	+++	+++	+++	+++	+++
Field CA2 (CA2)	+++	+++	+++	+++	+++	+++
Field CA3 (CA3)	+	+	+	+	+	+
Dentate gyrus (DG)	+	+	+/-	+/-	+	+
Entorhinal area (ENT)	+/-	+/-	+	+	+/-	+/-
Presubiculum / Subiculum (PRE/SUB)	+	+	+	+	+	+
Cortical subplate and cerebral nuclei						
Septohippocampal nucleus (SH)	+	+	+	+	+	+
Lateral septal nucleus, caudodorsal (LSc)	+++	+	+	+	+	+
Lateral septal nucleus, rostroventral (LSr)	+++	+	+	+	+	+
Bed nucleus of stria terminalis, principal nucleus (BSTpr)	++++	+++	+	+	+++	+++
Cortical amygdalar area (COA)	+++	+++	+	+	+++	+++
Medial amygdalar nucleus, posterodorsal (MEApd)	+++	+	+	+	+++	+++
Posterior amygdala (PA)	+++	+	+++	+	+++	+
Thalamus and Subthalamus						
Ventral posterior complex of the thalamus (VP)	+	+	+	+	+	+
Paraventricular nucleus of the thalamus (PVT)	+	+	+	+	+	+
Nucleus of reuniens (RE)	+/-	+/-	+	+	++	+
Subthalamic/ Parathalamic, caudal (STN/PSTN)	++	+	+	+	++	++
Medial geniculate complex (MG)	+	+	+	+	++	+
Hypothalamus						
Medial preoptic area, anterior (MPOa)	+	+	+	+	+	+

	Adult		Prepubertal			
	PND 56–70		PND 12		PND 21	
	Male	Female	Male	Female	Male	Female
Brain areas and nuclei						
Medial preoptic area, posterior (MPOp)	++++	++++	++++	++++	++++	++++
Suprachiasmatic nucleus (SCH)	++	+	+/-	+/-	+	+/-
Paraventricular hypothalamic nucleus (PVH)	+/-	+/-	-	-	-	-
Periventricular hypothalamic nucleus (PV)	+	+/-	-	-	-	-
Subparaventricular zone (SBPV)	+	+	++	++	+	+
Lateral hypothalamic area (LHA)	+/-	+/-	-	-	-	-
Arcuate hypothalamic nucleus (ARH)	++	+	+/-	+/-	+	+
Ventromedial hypothalamic nucleus, ventrolateral (VMHvl)	+	++	+	+	++	+
Tuberal nucleus (TU)	+	+	-	-	+	+
Dorsomedial nucleus of the hypothalamus (DMH)	+	-	-	-	+/-	-
Dorsal premammillary nucleus (PMd)	+	+	++	++	++	++
Ventral premammillary nucleus (PMv)	++++	++++	+++	+++	+++	+++
Supramammillary nucleus (SUM)	+	+/-	+	+	+	+/-
Midbrain						
Periaqueductal gray, ventrolateral (PAGvl)	+/-	+/-	+/-	+/-	+	+
Ventral tegmental area (VTA)	+/-	-	-	-	-	-
Red nucleus (RN)	+/-	-	-	-	+/-	-
Dorsal nucleus raphe (DR)	+/-	+/-	+/-	+/-	+	+
Pons and Medulla						
Pontine reticular nucleus (PRN)	+/-	+/-	+/-	+/-	+/-	+/-
Superior olivary complex (SOC)	-	-	+	+	+	+
Principal sensory nucleus of the trigeminal (PSV)	-	-	+	+/-	+	-
Parabrachial nucleus (PB)	+/-	+/-	-	-	-	-
Dorsal tegmental nucleus (DTN)	+	+	+	+	+	+
Facial motor nucleus (VII)	+	+/-	+	+	+	+
Cochlear nuclei (CN)	+/-	-	+	+	+	+
Vestibular Nucleus (VNC)	+/-	-	+	+	+	+
Nucleus ambiguus (AMB)	+/-	+/-	++	++	++	++
Hypoglossal nucleus (XII)	+	+	+	+	++	++
Nucleus of the solitary tract (NTS)	+/-	+/-	+/-	+/-	+/-	+/-
Dorsal motor nucleus of vagus nerve (DMX)	+	+	+	+	++	++
Circumventricular Organs						
Subfornical organ (SFO)	+/-	+	+	+	+/-	+/-
Area postrema (AP)	+/-	+/-	+/-	+/-	+	+